DRUG DEVELOPMENT

A molecular glue degrader of the WIZ transcription factor for fetal hemoglobin induction

Pamela Y. Ting[1]*, Sneha Borikar[1], John Ryan Kerrigan[1], Noel M. Thomsen[1], Eamon Aghania[1], Amelia E. Hinman[1], Alejandro Reyes[2], Nicolas Pizzato[2], Barna D. Fodor[2], Fabian Wu[2], Muluken S. Belew[1]†, Xiaohong Mao[1], Jian Wang[1], Shripad Chitnis[1], Wei Niu[1]‡, Amanda Hachey[1], Jennifer S. Cobb[1], Nikolas A. Savage[1], Ashley Burke[1], Joshiawa Paulk[1], Dustin Dovala[3], James Lin[3], Matthew C. Clifton[3], Elizabeth Ornelas[3], Xiaolei Ma[3]§, Nathaniel F. Ware[1], Carina C. Sanchez[1], John Taraszka[1], Remi Terranova[2], Judith Knehr[2], Marc Altorfer[2], S. Whitney Barnes[4], Rohan E. J. Beckwith[1]¶, Jonathan M. Solomon[1], Natalie A. Dales[1]#, Andrew W. Patterson[1], Jürgen Wagner[2], Tewis Bouwmeester[2], Glenn Dranoff[1]**, Susan C. Stevenson[1], James E. Bradner[1]*††

Sickle cell disease (SCD) is a prevalent, life-threatening condition attributable to a heritable mutation in β-hemoglobin. Therapeutic induction of fetal hemoglobin (HbF) can ameliorate disease complications and has been intently pursued. However, safe and effective small-molecule inducers of HbF remain elusive. We report the discovery of dWIZ-1 and dWIZ-2, molecular glue degraders of the WIZ transcription factor that robustly induce HbF in erythroblasts. Phenotypic screening of a cereblon (CRBN)–biased chemical library revealed WIZ as a previously unknown repressor of HbF. WIZ degradation is mediated by recruitment of WIZ (ZF7) to CRBN by dWIZ-1, as resolved by crystallography of the ternary complex. Pharmacological degradation of WIZ was well tolerated and induced HbF in humanized mice and cynomolgus monkeys. These findings establish WIZ degradation as a globally accessible therapeutic strategy for SCD.

Sickle cell disease (SCD) arises from a missense mutation in the β-globin gene (*HBB*) that predisposes hemoglobin to polymerization and vaso-occlusive sickling of erythrocytes (*1*). Hereditary persistence or pharmacologic induction of γ-globin (*HBG1* or *HBG2*, henceforth *HBG1/2*) expression leads to increases in fetal hemoglobin (HbF) that biophysically oppose hemoglobin polymerization (*2*, *3*).

The most effective oral therapy for SCD is presently hydroxyurea (HU), which confers disease-modifying benefits and improved survival (*4*). The clinical efficacy of HU arises in part from modest reactivation of HbF (median ~15% of total Hb) (*4*, *5*), an indirect consequence of inhibiting ribonucleotide reductase and thus DNA synthesis. However, broad use of HU is limited by bone marrow suppression and a requirement for close laboratory monitoring. Further underscoring the potential of HbF reactivation are recent accounts by our group and others (*6*–*8*) of successful myeloablative transplantation of autologous hematopoietic stem and progenitor cells (HSPCs) genetically modified to disrupt repressors of *HBG1/2*. Regrettably, substantial challenges exist for HSPC therapies to reach most SCD patients, who live in medically underserved communities and low- and middle-income countries. Safe, efficacious, and globally accessible HbF-inducing medicines therefore remain an important unmet need.

Human genetics and functional genetic screens have enumerated a number of promising protein targets for *HBG1/2* derepression, including BCL11A, KLF1, c-Myb, and LRF (*3*, *9*). Despite increasingly compelling mechanistic validation, these transcription factors (TFs) function by protein-protein interaction and thus remain challenging to inhibit using conventional approaches in drug discovery (*10*). Leveraging recent mechanistic characterization of phthalimide medicines as serendipitous, cereblon (CRBN)–dependent degraders of IKZF1 and IKZF3 (*11*–*16*), we hypothesized the plausible degradation of zinc finger (ZF)–containing TFs by chemically distinct molecular glue degraders. Therefore, we elaborated a large library of CRBN-biased ligands for study in target-directed and phenotypic drug discovery campaigns.

Discovery of WIZ as regulator of HbF induction by phenotypic screening

To identify small molecules that induce HbF, we developed a high-throughput screening assay in primary human CD34$^+$ derived erythroblasts to measure proliferation, differentiation, and HbF expression by flow cytometry after a 13-day culture (fig. S1A). Known HbF inducers, such as HU, decitabine (DNA methyltransferase inhibitor), and UNC0642 (EHMT1 and EHMT2 lysine methyltransferase inhibitor) (*17*, *18*) induced HbF but exhibited undesirable antiproliferative effects (fig. S1B).

Using this assay, we next screened a library of 2814 CRBN-biased molecules (Fig. 1, A to C). Induction of HbF was observed in 7.4% of tested molecules (Fig. 1C), including the Food and Drug Administration (FDA)–approved agent, pomalidomide, which has been reported preclinically to induce HbF (*19*, *20*). Multiplexed primary screening and dose-response follow-up assays identified antidifferentiation or antiproliferative activity for almost all assay positives, including pomalidomide, which halted further characterization. Three compounds increased the percentage of HbF-positive cells while sparing erythroblast proliferation and differentiation, and one compound—compound C (Fig. 1B)—was prioritized after further characterization because of superior absorption, distribution, metabolism, and excretion (ADME) properties. Compound C increased the percentage of HbF-positive cells with a half-maximal effective concentration (EC_{50}) of 100 nM while sparing erythroblast proliferation and differentiation (Fig. 1, D and E, and table S1). HbF induction was not observed in erythroblasts rendered CRBN-deficient by CRISPR-Cas9 (Fig. 1F and fig. S2A), which suggests that compound C acts through a protein degradation–dependent mechanism to induce HbF.

To identify potential targets of compound C, we performed an unbiased analysis of protein stability by mass spectrometry. Primary human erythroblasts were treated with 10 μM compound C or dimethyl sulfoxide (DMSO) control for 6 hours. From 8960 quantified proteins, the most significantly down-regulated protein was the WIZ TF (2.6-fold, $P = 0.0001$; Fig. 2A). Compound C proved selective for WIZ, with no additional proteins depleted more than twofold. Compound C did not affect the abundance of known HbF regulators (table S2) and was also selective over known lenalidomide targets IKZF1 (fig. S2B) and CK1α (table S2). Notably, no change in the expression of *WIZ* mRNA was observed by reverse transcription quantitative polymerase chain reaction (RT-qPCR) (fig. S2C), which supports a posttranscriptional effect on WIZ abundance. A potent dose-dependent effect of compound C on WIZ protein level was established by immunoblot in 293T cells transduced with a WIZ-overexpression construct (Fig. 2B) and confirmed by measuring the effect on endogenous WIZ by flow cytometry in primary human erythroblasts [half-maximal degradation concentration (DC_{50}) of 13 nM; Fig. 2C and fig. S2D]. We renamed this chemical probe dWIZ-1.

WIZ is a chromatin-associated TF that localizes to promoters, enhancers, and insulators (*21*, *22*). The emerging literature identifies structural and biological characteristics supporting WIZ as a putative HbF gene control factor. WIZ associates with at least two cohesin-CTCF complexes to influence DNA

[1]Novartis Biomedical Research, Cambridge, MA, USA. [2]Novartis Biomedical Research, Basel, Switzerland. [3]Novartis Biomedical Research, Emeryville, CA, USA. [4]Novartis Biomedical Research, San Diego, CA, USA.
*Corresponding author. Email: pamela.ting@novartis.com (P.Y.T.); jbradner@gmail.com (J.E.B.)
†Present address: Notch Therapeutics, Toronto, ON, Canada.
‡Present address: Arvinas, New Haven, CT, USA.
§Present address: Terremoto Biosciences, San Francisco, CA, USA.
¶Present address: Neomorph, San Diego, CA, USA.
#Present address: Odyssey Therapeutics, Cambridge, MA, USA.
**Present address: Dana Farber Cancer Institute, Boston, MA, USA.
††Present address: Amgen, Thousand Oaks, CA, USA.

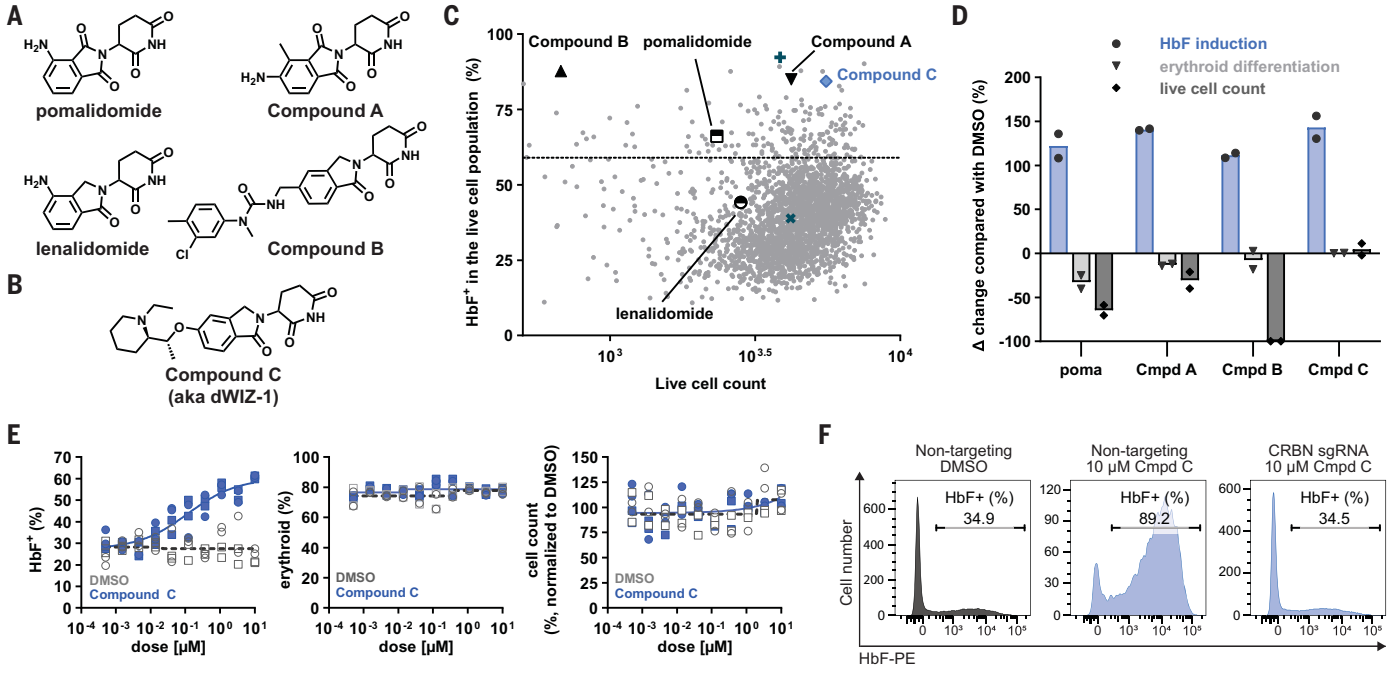

Fig. 1. Discovery of a CRBN-based small-molecule inducer of HbF. (**A**) Structures of reference compounds and selected hits described in (C) and (D). (**B**) Structure of compound C. (**C**) Results of primary screen. Each point represents a separate compound. "x" denotes the average of DMSO control wells, and "+" denotes the average of UNC0642 positive control wells. In total, 7.4% of compounds induced HbF (defined as >3 SDs over mean of DMSO controls and indicated by the dotted line). (**D**) Hit reconfirmation data from selected compounds at 10 μM. HbF induction (HbF^+ cells in the $CD71^+CD235a^+$ population), erythroid differentiation (%$CD71^+CD235a^+$), and live cell count were assessed by flow cytometry. (**E**) Dose-response curves based on flow cytometry analysis of HbF^+ cells ($CD71^+CD235a^+$), erythroid differentiation ($CD71^+CD235a^+$), and cell count on day 7 of erythroid differentiation. n = 2 donors (squares versus circles) with two replicates each. (**F**) Representative flow cytometry analysis of HbF staining ($CD71^+CD235a^+$) on day 7 of differentiation.

loop integrity (*21*–*23*), establishing a plausible impact on the globin locus control region (*24*). Further, WIZ associates stably with the C-terminal binding protein (CtBP) corepressor complex, facilitating recruitment of EHMT1 and EHMT2 (EHMT1/2) (*25*, *26*), which have been linked enzymatically to HbF induction (*17*, *18*). WIZ is broadly expressed in multiple tissues, and reported transcriptional profiling data identify robust *WIZ* and *CRBN* expression throughout erythropoiesis (fig. S2E) (*27*).

Because small-molecule probes may have off-target consequences, we tested the effect of WIZ loss on HbF using CRISPR-Cas9 in primary human erythroblasts from healthy donors (fig. S3, A and B). *WIZ* knockout (KO) using two independent single-guide RNAs (sgRNAs) significantly elevated the proportion of γ-globin mRNA (fig. S3C), HbF^+ cells (Fig. 2D), and total HbF (Fig. 2E and fig. S3D). Although γ-globin transcript expression increased (fig. S3E), the abundance of α-, β-, δ-, and ε-globin mRNA remained unchanged (fig. S3, F to I). Cell surface phenotyping using anti-CD71 and anti-CD235a indicated normal erythroid differentiation in WIZ-deficient cells (fig. S3, J and K).

To assess the effect of WIZ depletion on hematopoiesis and developing erythroblasts in vivo, we used an established humanized xenotransplantation model that supports human erythropoiesis in the bone marrow (*28*). Using CRISPR-Cas9, we knocked out *WIZ* with two independent sgRNAs in healthy human donor $CD34^+$ HSPCs and generated two negative control groups using either a nontargeting or a safe-targeting sgRNA (*29*). We transplanted NBSGW mice (*30*) and assessed engraftment, multilineage differentiation, and HbF induction in the peripheral blood and bone marrow after 16 weeks. Early and late engraftment was comparable between *WIZ*-targeted and control groups (Fig. 2F and fig. S4A). WIZ-deficient HSPCs repopulated the bone marrow (Fig. 2G) and reconstituted normal distributions of B, T, myeloid (Fig. 2H), and erythroid lineages (Fig. 2I). Similar editing frequencies were observed pre- and posttransplantation (fig. S4, B and C). Notably, WIZ-deficient erythroblasts derepressed HbF (Fig. 2, J to L), validating WIZ as a previously unrecognized repressor of HbF in vivo.

Characterization of dWIZ-1 as a molecular glue degrader of WIZ

Although structural characterization of WIZ has not been previously reported, sequence analysis and modeling by AlphaFold suggest 11 putative ZFs, five of which arise as paired ZFs (fig. S5A). By analogy to the ZF-dependent recruitment of IKZF1 to the CRBN-DDB1 ubiquitin ligase complex (*12*), we tested the thesis that dWIZ-1 recruits WIZ to CRBN-DDB1 to trigger targeted protein degradation. Seven of the WIZ ZFs contain the CxxCG motif present in other known CRBN neosubstrates (*31*).

We first assessed compound-induced WIZ and CRBN association using a cell-based NanoBiT protein-protein recruitment assay, in which bioluminescence increases as SmBiT-CRBN is brought into proximity to LgBiT-WIZ. As shown in fig. S5B, dWIZ-1 increases CRBN-WIZ association with an EC_{50} of 547 nM. Consequent proteasome-dependent degradation of WIZ was assessed in a HiBiT-tagged WIZ-overexpression cell line by treatment with dWIZ-1 in the presence or absence of a neddylation inhibitor (MLN4924), a ubiquitin activating enzyme inhibitor (MLN7243), and a proteosome inhibitor (bortezomib). Treatment with each ubiquitin-proteasome pathway inhibitor rescued WIZ stability (fig. S5C), consistent with E3-dependent proteasomal degradation.

To identify the dWIZ-1 degron in the WIZ open reading frame, we studied ZF7 to ZF10, which are all present in the most highly expressed isoforms in human primary erythroblasts (fig. S5D). We introduced point mutations

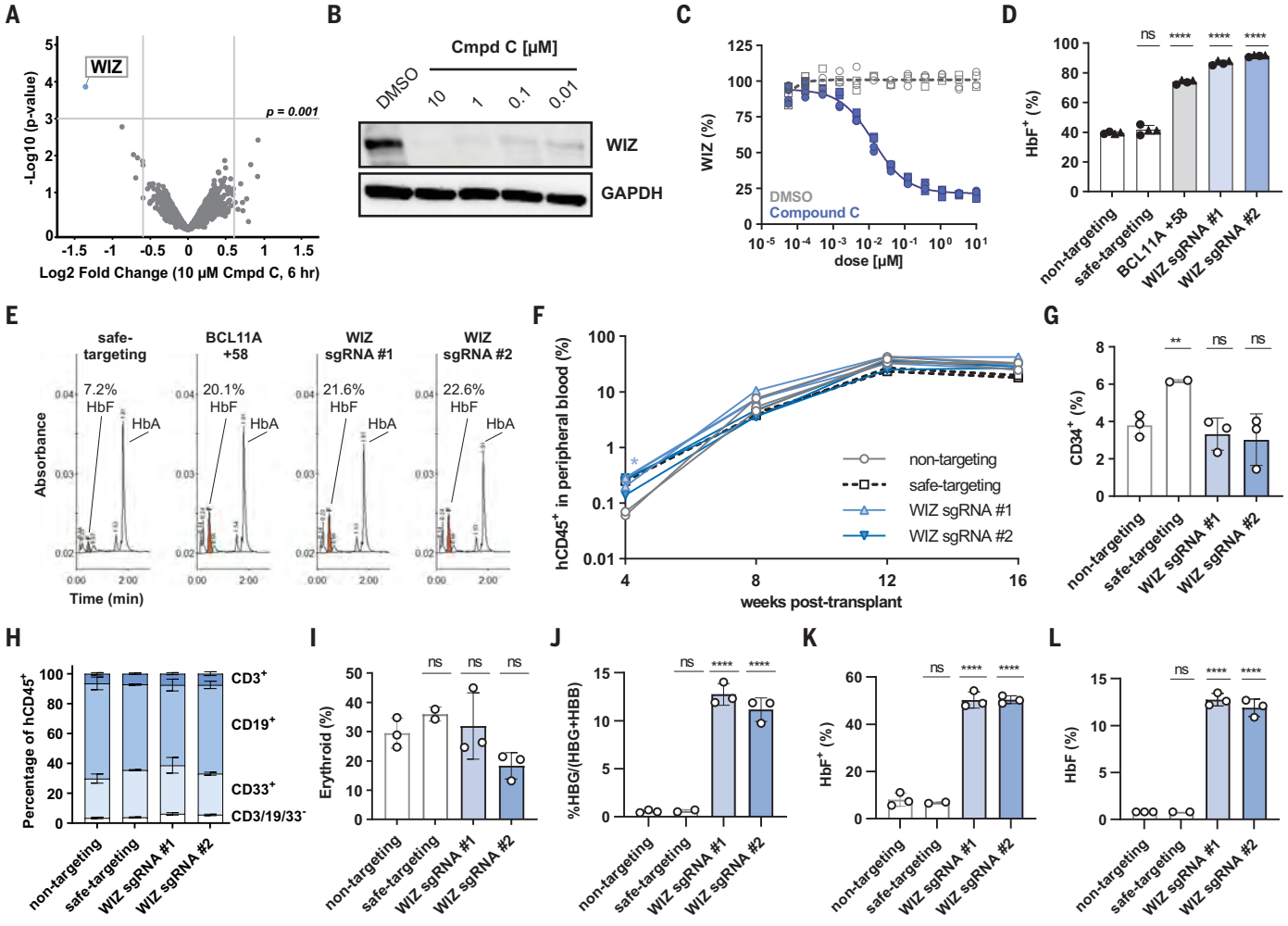

Fig. 2. Target identification and characterization of WIZ as a negative regulator of HbF expression. (**A**) Quantitative proteomics profiling of primary human erythroblasts treated for 6 hours with 10 μM compound C versus DMSO (protein FDR < 1%; $n = 2$ biological replicates per treatment). Log_2(fold change) difference between means of treated versus DMSO plotted against P values calculated using Limma. Lines in the plot indicate significant cutoffs: $P < 0.001$ and absolute log_2(fold change) > 0.6. (**B**) Immunoblot analysis of whole-cell lysates from HiBiT-tagged WIZ-overexpression 293T cells treated with indicated concentrations of compound C for 24 hours. GAPDH, glyceraldehyde-3-phosphate dehydrogenase. (**C**) Dose-response curve based on flow cytometry analysis of WIZ expression in $CD71^+$ primary human erythroblasts after 24 hours of treatment. $n = 2$ donors (squares versus circles) with two replicates each. (**D**) Flow cytometry analysis of HbF^+ cells ($CD71^+CD235a^+$) on differentiation day 14 ($n = 2$ donors with two replicates each). Data are presented as means and SDs, with different symbols indicating the different donors. (**E**) Representative HPLC analysis on differentiation day 18. HbA, adult hemoglobin. (F to L) $n =$ 3 mice in nontargeting and WIZ groups; $n = 2$ safe-targeting. (**F**) Human $CD45^+$ chimerism in peripheral blood from NBSGW mice at indicated weeks posttransplantation. The asterisk indicates an adjusted P value of 0.014 for nontargeting versus WIZ sgRNA no. 1 at 4 weeks. All other comparisons between nontargeting and other groups were not statistically significant using two-way analysis of variance (ANOVA) and Dunnett's multiple comparisons. (G to L) All analyses are from bone marrow 16 weeks posttransplantation. Data are presented as individual animals with the mean. Statistical significance compared with the nontargeting group was determined by one-way ANOVA with Dunnett's multiple comparisons. $P > 0.05$, not significant (ns); $^{**}P \le 0.01$; $^{****}P \le 0.0001$. (**G**) $CD34^+$ HSPCs expressed as a percentage of human $CD45^+$. (**H**) Human T cell ($CD3^+$), B cell ($CD19^+$), myeloid ($CD33^+$), and other cell types ($CD3^-/CD19^-/CD33^-$). Adjusted $P = 0.006$ for B cell population in nontargeting versus WIZ sgRNA no. 1. (**I**) $CD235a^+$ erythroid cells expressed as a percentage of $hCD45^-moCD45^-$. (**J**) RT-qPCR with γ-globin mRNA presented as a percentage of total γ- and β-globin transcript. (**K**) Summary of flow cytometry analysis of HbF expression in $moCD45^-hCD45^-CD71^+CD235a^+$. (**L**) HbF level measured by HPLC from hemolysates of enriched bone marrow $CD235a^+$ cells. The HbF levels in the nontargeting and safe-targeting groups were less than the lower limit of quantitation (LLOQ) of 0.8% and are graphed as 0.8%.

targeting a glycine residue in each β-hairpin loop that has proven critical for binding of other CRBN neosubstrates (*13*, *14*). A G876N mutation in ZF7 fully rescued WIZ degradation in a HiBiT-tagged overexpression cell line, whereas similar mutations in ZF8 (G1049N), ZF9 (G1233N), ZF10 (G1403N), and the combination G1049N/G1233N/G1403N had no effect on the potency or depth of WIZ degradation (Fig. 3A and fig. S5E). Together, these data support WIZ(ZF7) as the primary ZF involved in ternary complex formation, functionally confirmed by dose-dependent recruitment of WIZ(ZF7) to CRBN by dWIZ-1 in a NanoBiT expression system (fig. S5F).

To confirm direct WIZ ZF binding in vitro, we assayed the binding of recombinant WIZ ZFs (fig. S6A) to the DDB1:CRBN:dWIZ-1 complex using surface plasmon resonance (SPR). We observed binding of WIZ(ZF7) to the DDB1:CRBN:dWIZ-1 complex with an affinity of 3.5 μM ± 0.6 μM (Fig. 3B and fig. S6B). Notably, no binding

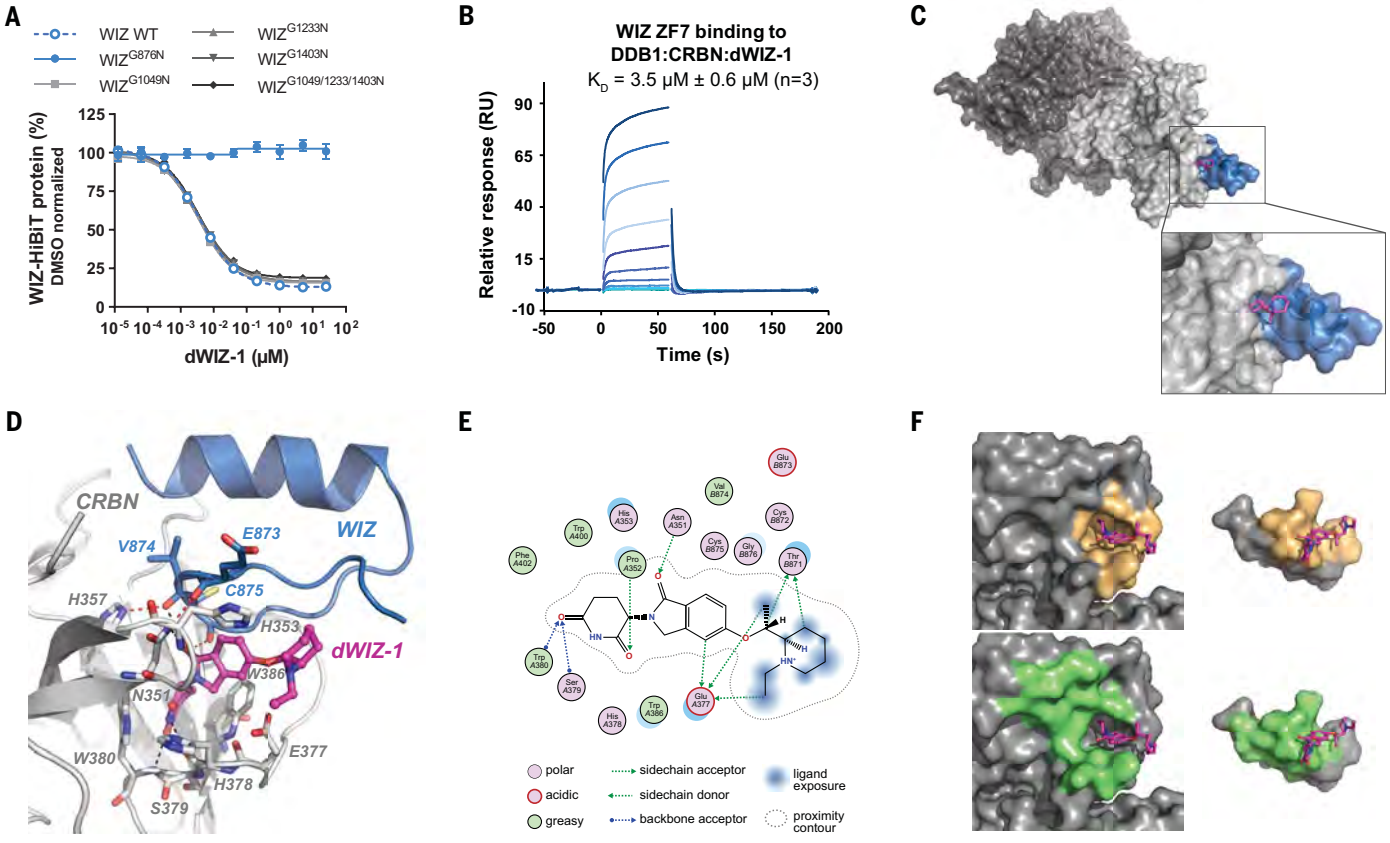

Fig. 3. WIZ is recruited to CRBN through ZF7. (**A**) WIZ HiBiT-tagged protein levels were measured after 18 hours treatment in the presence of increasing doses of dWIZ-1 in 293T cells. Data are means ± SDs of three replicates. (**B**) Representative SPR data for the binding of WIZ ZF7 to the DDB1:CRBN:dWIZ-1 complex. The steady-state binding affinity value represents the average of three independent experiments. (**C**) Structure of DDB1ΔBPB:CRBNΔ67:WIZ(ZF7) bound to dWIZ-1. dWIZ-1 (pink) creates a tight protein-protein interaction between CRBN (gray) and WIZ (blue). (**D**) Ligand binding pocket for DDB1ΔBPB:CRBNΔ67:WIZ(ZF7) bound to dWIZ-1 determined at 3.15 Å. Hydrogen bonds are shown as dashed lines to dWIZ-1 (black) and between CBRN and WIZ(ZF7) (red). (**E**) LigPlot for dWIZ-1 generated by molecular operating environment (MOE). (**F**) Binding of the molecular glue creates additional buried surface area at the protein-protein interface between CRBN and WIZ(ZF7). Buried surface from the binding of dWIZ-1 (orange) is compared with the buried surface between CRBN and WIZ (green). Single-letter abbreviations for the amino acid residues are as follows: A, Ala; C, Cys; D, Asp; E, Glu; F, Phe; G, Gly; H, His; I, Ile; K, Lys; L, Leu; M, Met; N, Asn; P, Pro; Q, Gln; R, Arg; S, Ser; T, Thr; V, Val; W, Trp; and Y, Tyr.

(up to 10 μM) of WIZ(ZF7) to DDB1:CRBN was observed in the absence of dWIZ-1, and no binding was observed with DDB1 alone in the presence of dWIZ-1 (fig. S6C), demonstrating both compound- and CRBN-dependent binding. By contrast, neither WIZ(ZF8/ZF9) nor WIZ(ZF10) demonstrated binding to the DDB1:CRBN:dWIZ-1 complex (fig. S6D).

The structural basis of neosubstrate recruitment was determined by x-ray crystallography of DDB1ΔBPB:CRBNΔ67:WIZ(ZF7), in the presence of dWIZ-1 (3.1 Å; Fig. 3C, fig. S7A, and table S3). The dWIZ-1 ligand appears bound between CRBN and WIZ(ZF7) as a ternary complex (fig. S7B). CRBN adopts the closed conformation (*32*), positioning the N-terminal domain near the glutarimide recognition pocket. The complex is reminiscent of previously determined CRBN ternary complexes, where the β-hairpin glycine (G876) accommodates the phthaloyl ring and allows the glutarimide ring to bind into the tri-tryptophan pocket (fig. S7C). dWIZ-1 coordinates a series of hydrogen bond interactions to CRBN using N351, H378, W380, and W400. WIZ(ZF7) establishes an additional hydrogen bond with dWIZ-1 using V874 (Fig. 3, D and E). dWIZ-1 creates hydrogen bond interactions between CRBN:WIZ(ZF7) including the pairs N351:E873, H357:V874, and W400:C875. This "molecular glue" type interaction creates a tightly buried surface area between CRBN and WIZ(ZF7), with only the ethyl-piperidine partially exposed to solvent (Fig. 3C). The calculated buried surface area between CRBN and WIZ(ZF7) is 413.8 Å^2, that between CRBN and dWIZ-1 is 305 Å^2, and that between WIZ(ZF7) and dWIZ-1 is 152 Å^2 (Fig. 3F) (*33*, *34*). Steric clashes with Ikaros (Q146) and CK1α (I35) offer one possible explanation for the selectivity of dWIZ-1 against these known CRBN off-targets (fig. S7, C and D). Collectively, these data lend strong support to the thesis that dWIZ-1 induces HbF expression by direct binding to CRBN and subsequent recruitment and proteasomal degradation of WIZ through WIZ(ZF7).

A drug-like degrader of WIZ for pharmacologic target validation

To extend the study of WIZ degradation and HbF induction in vivo, lead optimization efforts identified a near chemical analog, named dWIZ-2, where the chiral methyl of dWIZ-1 is removed, resulting in improved pharmacokinetic (PK) properties (Fig. 4A, table S1, and fig. S8A). dWIZ-2 potently degraded WIZ in primary human erythroblasts in vitro (fig. S8B), and unbiased proteomic analysis identified only a small number of additional proteins depleted (fig. S8C and table S4). Treatment of primary human erythroblasts from healthy donors led to dose-dependent induction of HbF (fig. S8D), with no adverse effect on erythroid differentiation or proliferation (fig. S8, E and F) in contrast to HU, which markedly decreased cell viability

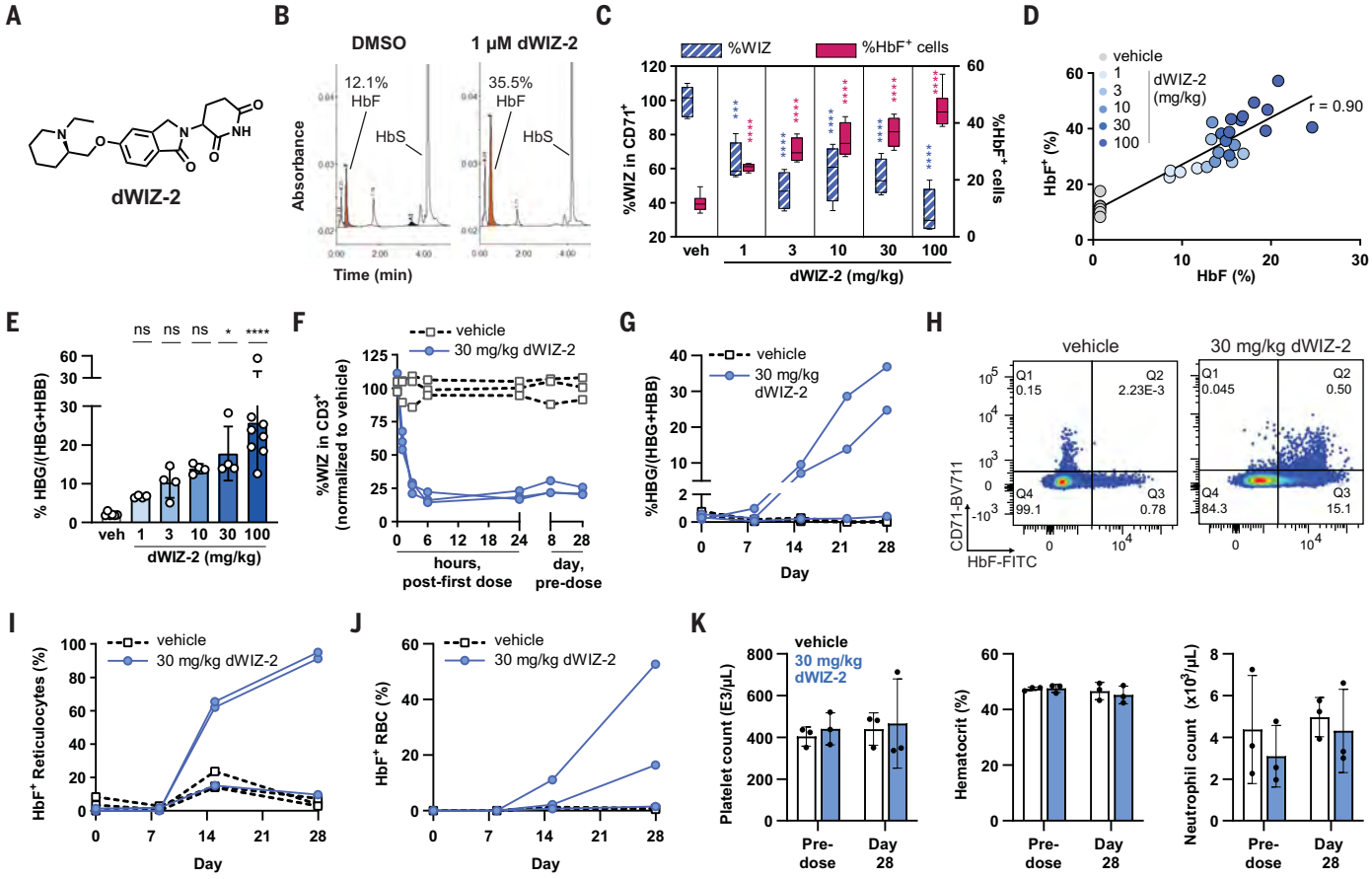

Fig. 4. An optimized molecular glue degrader of WIZ for HbF induction. (**A**) Structure of dWIZ-2. (**B**) Representative HPLC analysis of SCD patient–derived primary human erythroblasts on differentiation day 18. HbS, sickle-cell hemoglobin. (C and D) Humanized NBSGW mice were dosed by mouth once per day (po/qd) with vehicle (n = 6), or 1 (n = 4), 3 (n = 4), 10 (n = 4), 30 (n = 4), or 100 (n = 8) mg/kg dWIZ-2 for 21 days. (**C**) Summary of flow cytometry analysis of WIZ and HbF expression in moCD45$^-$hCD45$^-$CD71$^+$ bone marrow cells. Statistical significance compared with vehicle was determined by one-way ANOVA with Dunnett's multiple comparisons. ***P = 0.0003; ****$P \leq 0.0001$. (**D**) Pearson correlation between HbF$^+$ cells, as assessed in (C) with HbF level measured by HPLC from hemolysates of enriched bone marrow CD235a$^+$ cells. Each dot represents the results from an individual mouse. All vehicle animals were less than LLOQ 0.8% HbF. (**E**) γ-globin mRNA is presented as a percentage of total β-like globin transcript. Data are presented as individual animals with the means and SDs. Statistical significance compared with vehicle was determined by one-way ANOVA with Dunnett's multiple comparisons. $P > 0.05$, ns; *$P \leq 0.05$; ****$P \leq 0.0001$. (F to K) Cynomolgus monkeys were dosed po/qd with vehicle or 30 mg/kg dWIZ-2 for 28 days. n = 3 monkeys per group. Each point or series of connected points represents the results from an individual monkey. (**F**) Summary of flow cytometry analysis of WIZ expression in peripheral blood CD3$^+$ cells. (**G**) RT-qPCR of γ-globin mRNA in peripheral blood, as a percentage of total γ- and β-globin transcript. (**H**) Representative flow cytometry analysis of HbF staining in peripheral blood red blood cells and CD71$^+$ reticulocytes on day 28. (**I** and **J**) Summary of HbF flow cytometry analysis in peripheral blood CD71$^+$ reticulocytes (I) and red blood cells (RBCs) (J). (**K**) Peripheral blood hematology parameters. Data are presented as means and SDs.

(fig. S8G). We also observed dose-dependent WIZ degradation in CD34$^+$-derived erythroblasts from three SCD patients (fig. S8H). Treatment of SCD-derived erythroblasts with dWIZ-2 increased both the percentage of HbF-expressing cells (fig. S8I) as well as total HbF from a mean baseline of 17% in vehicle-treated samples to 45% in 10 μM dWIZ-2–treated samples (Fig. 4B and fig. S8J). dWIZ-2–treated cells displayed normal erythroid differentiation and maturation as assessed by the fraction of CD71$^+$CD235a$^+$ erythroblasts (fig. S8K) and enucleated red cell precursors (fig. S8L).

After oral administration in mice, dWIZ-2 displays rapid absorption, with peak concentration at 1 to 2 hours after dose and moderate bioavailability (F = 13 to 41%) (table S1). Because of known species-specific differences in human and murine CRBN (*11*), we studied the in vivo activity of dWIZ-2 in human HSPCs transplanted into immunocompromised mice. NBSGW mice humanized with CD34$^+$ HSPCs from healthy human donors were orally dosed once daily with dWIZ-2 during weeks 16 to 18 posttransplantation (fig. S9A). Oral treatment with dWIZ-2 was well tolerated up to 100 mg/kg as assessed by body weight compared with vehicle control (fig. S9B). dWIZ-2 exposure resulted in robust and dose-dependent WIZ degradation (mean 65%) accompanied by an increase in the proportion of HbF$^+$ human erythroblasts in the bone marrow compared with vehicle control (42% versus 10%; $P < 0.0001$) (Fig. 4C). The increase in HbF$^+$ human erythroblasts positively correlated with fractional HbF expression as measured by high-performance liquid chromatography (HPLC) (r = 0.9; 19% versus <0.8%; Fig. 4D) and was primarily driven by an increase in γ-globin mRNA transcript (26% versus 2%; Fig. 4E and fig. S9C).

To extend the assessment of HbF induction in vivo, we orally dosed naïve healthy cynomolgus monkeys with 30 mg/kg per day dWIZ-2 or vehicle control for 28 days. Antecedent PK study of dWIZ-2 in monkeys established

favorable PK characteristics after oral administration, with rapid absorption (peak concentration at 1 to 2 hours), excellent oral bioavailability (F = 72%), and a long elimination half-life ($T_{1/2}$ = 12 to 16 hours) (fig. S10A). After the first dose of dWIZ-2, rapid (<6 hours), deep (>75%), and durable (>24 hours) WIZ degradation was detected in the peripheral blood in $CD3^+$ peripheral blood mononuclear cells (PBMCs) by flow cytometry (Fig. 4F). Whole-blood measurement of *HBG* transcript (*35*) was used to measure initial HbF response. Elevation of γ-globin mRNA was detected in the blood at day 15, which continued to increase at day 28 (median 25%, 3 to 37% in individual animals; Fig. 4G and fig. S10, B and C). Peripheral detection of γ-globin mRNA coincided with the increasing appearance of HbF-expressing reticulocytes in the periphery on day 15, reaching >90% HbF^+ reticulocytes on day 28 in two of three animals treated with 30 mg/kg dWIZ-2 (Fig. 4, H and I, and fig. S10D). F-cells were not observed in most animals on day 15 but were present in the periphery on day 28, consistent with the maturation of HbF^+ reticulocytes to HbF^+ red blood cells (Fig. 4J). We found consistently across all measures of HbF that one monkey in the 30 mg/kg per day group was a nonresponder. Although this animal demonstrated comparable dWIZ-2 exposure and WIZ degradation to that in the other animals, the increase in γ-globin mRNA was roughly two orders of magnitude lower than that observed in the other two monkeys and did not translate to a significant increase in F-retics or F-cells assessed by flow cytometry. Notably, HbF induction was achieved without an impact on measured platelets, hematocrit, or neutrophils (Fig. 4K).

To characterize the therapeutic index of WIZ degradation more fully in monkeys, we assessed clinical toxicology associated with a high-dose exposure to dWIZ-2 for 28 days (300 mg/kg per day). No adverse signs or symptoms were observed clinically in dWIZ-2–treated animals, including stable body weight (fig. S10E). Clinical pathology failed to identify dWIZ-2–associated changes in measured blood counts, serum chemistries, or examined tissue histology.

WIZ binds genome-wide and supports repressive methylation of chromatin

To characterize the effect of dWIZ-2 on WIZ binding, chromatin structure, and transcription, we conducted genome-wide cleavage under targets and release using nuclease (CUT&RUN) and transcriptome assessments. WIZ CUT&RUN in primary human erythroblasts identified 99,975 WIZ binding sites: 32% at CTCF binding sites, 24% in gene bodies, 21% within intergenic regions, 12% at promoters, and 11% localized to enhancers (Fig. 5A). Reciprocally, WIZ occupies 96% of CTCF binding sites, 77% of enhancer elements, and 60% of promoters (Fig. 5B). Of the 12,399 promoters bound by WIZ, 85% (10,553) feature histone acetylation as measured by H3K9ac CUT&RUN, which suggests that WIZ principally localizes to euchromatin. Integrating these experimental measurements with published erythroblast Hi-C data (*36*) confirmed that 77% of WIZ enrichment peaks localize to active chromatin three-dimensional (3D) compartments (Fig. 5C).

Sequence analysis of WIZ-enriched sites did not identify a singular consensus binding site. Rather, WIZ principally localizes to sequences predicted to bind CTCF, GATA TFs, and REST-NRSF. Notably, the motifs of well-known regulators of the β-globin locus, such as BACH2, MYB, NF-Y, KLF1, and BCL11A, were also enriched within WIZ peaks (Fig. 5D).

Within the β-globin locus, we observed 12 WIZ-enriched sites, two of which overlap CTCF binding sites at regional boundaries. All five hypersensitive sites of the 5′ locus control region (LCR) featured WIZ enrichment (Fig. 5E). WIZ enrichment was also observed at the promoters of fetal globin gene *HBG2*, adult globin genes (*HBB* and *HBD*), and the noncoding gene *BGLT3*. WIZ enrichment sites within the β-globin locus overlapped with binding sites of other key TFs implicated in globin regulation such as GATA1, KLF1, TAL1, and BCL11A (fig. S11A).

To explore the function of WIZ at the β-globin locus, we leveraged the utility of dWIZ-2 as a chemical probe, performing dynamic measurements of chromatin states and transcriptional output acutely after drug treatment of cultivated primary human erythroblasts. By pharmacodynamic CUT&RUN, dWIZ-2 treatment decreased dynamic WIZ binding genome-wide by 38% on day 2 of differentiation and by 49% on day 4 (fig. S11B). Within the β-globin locus, WIZ binding reduction upon dWIZ-2 treatment ranged from 27 to 71% and from 41 to 71% at differentiation days 2 and 4, respectively (Fig. 5E).

Because WIZ is known to bind the H3K9 methyltransferases EHMT1/2, we measured the dynamic effect of dWIZ-2 treatment on H3K9me2 globally and locally at the β-globin locus. As measured by mass spectrometry, the percentage of total measured histone H3 peptides (amino acids 9 to 17) marked with K9me2 decreased from 34.4% in DMSO-treated cells to 29.1% in cells treated with dWIZ-2 for 7 days at 10 μM. This reduction translated into a 15.4% relative decrease of H3K9me2 upon dWIZ-2 treatment (Fig. 5F and fig. S11C).

To explore the regional impact on heterochromatin, we performed H3K9me2 CUT&RUN in erythroblasts treated with dWIZ-2. Genome-wide, H3K9me2 loss was significantly more pronounced in regions with higher WIZ binding density (Fig. 5G and fig. S11, D and G). Consistent with these observations, we observed a significant loss of H3K9me2-marked chromatin in the β-globin locus (Fig. 5E). The regional losses of H3K9me2 were consistently reproduced both in erythroblasts treated with dWIZ-1 and when knocking out *WIZ* in erythroblasts (fig. S11, E to G).

Having principally characterized the effect of dWIZ-2 on the expression of γ-globin, we next examined the impact on global gene expression. Primary human erythroblasts were treated with dWIZ-2 for 24 hours or 7 days (10 μM), and differential transcription was assessed by RNA sequencing (RNA-seq). In total, 39 genes were differentially expressed on culture day 1 and 407 affected genes on day 7 [absolute $\log_2$ fold change > 1; 10% false discovery rate (FDR); Fig. 5, H and I, and fig. S11H]. Of these 407 differentially expressed genes, 293 were up-regulated (72%) consistent with WIZ function as a transcriptional repressor. Among the up-regulated genes was the long noncoding RNA (lncRNA) *BGLT3* ($\log_2$ fold change = 1.3; $P = 9.9 \times 10^{-10}$), which has previously been implicated in γ-globin regulation (*37*). Notably, 336 of 407 affected genes (83%) were comparably affected by WIZ loss by CRISPR KO at the same time point (Fig. 5J), which reports favorably on the use of dWIZ-2 as a mechanistic chemical probe.

Further supporting the link between EHMT1/2 and WIZ, 371 (91%) of the genes differentially expressed upon dWIZ-2 treatment had a directionally consistent fold change when treating with the EHMT1/2 inhibitor UNC0642 (Fig. 5K). Genomic regions with pronounced H3K9me2 losses upon dWIZ-2 treatment also consistently lost H3K9me2 upon treatment with UNC0642 (fig. S11, G and I). Conversely, treatment with dWIZ-2 had minimal effects on H3K9ac levels, with only 3% of the peaks showing significant changes in signal (fig. S11J). Genes and H3K9ac peaks that showed increased signals upon dWIZ-2 treatment tended to occur within regions losing H3K9me2 (fig. S11, K and L). Consistent with a derepressive effect of dWIZ-2 within the β-globin locus, we observed an increase in H3K9ac enrichment at the *HBG1* and *HBG2* promoters (more than twofold increase; $P < 10^{-10}$) (fig. S11, M and N). Taken together, these findings demonstrate WIZ binding within the β-globin locus and establish WIZ as a negative regulator of fetal globin expression and a positive regulator of repressive H3K9 dimethylation maintenance.

Discussion

SCD remains a profound, global unmet medical need. Presently, SCD affects 7.4 million people worldwide and is estimated to be increasing in prevalence, with more than half a million children born with SCD each year. Despite meaningful advances in the care of SCD patients and a detailed understanding of pathobiology, total disease mortality is also increasing to an estimated 376,000 patients

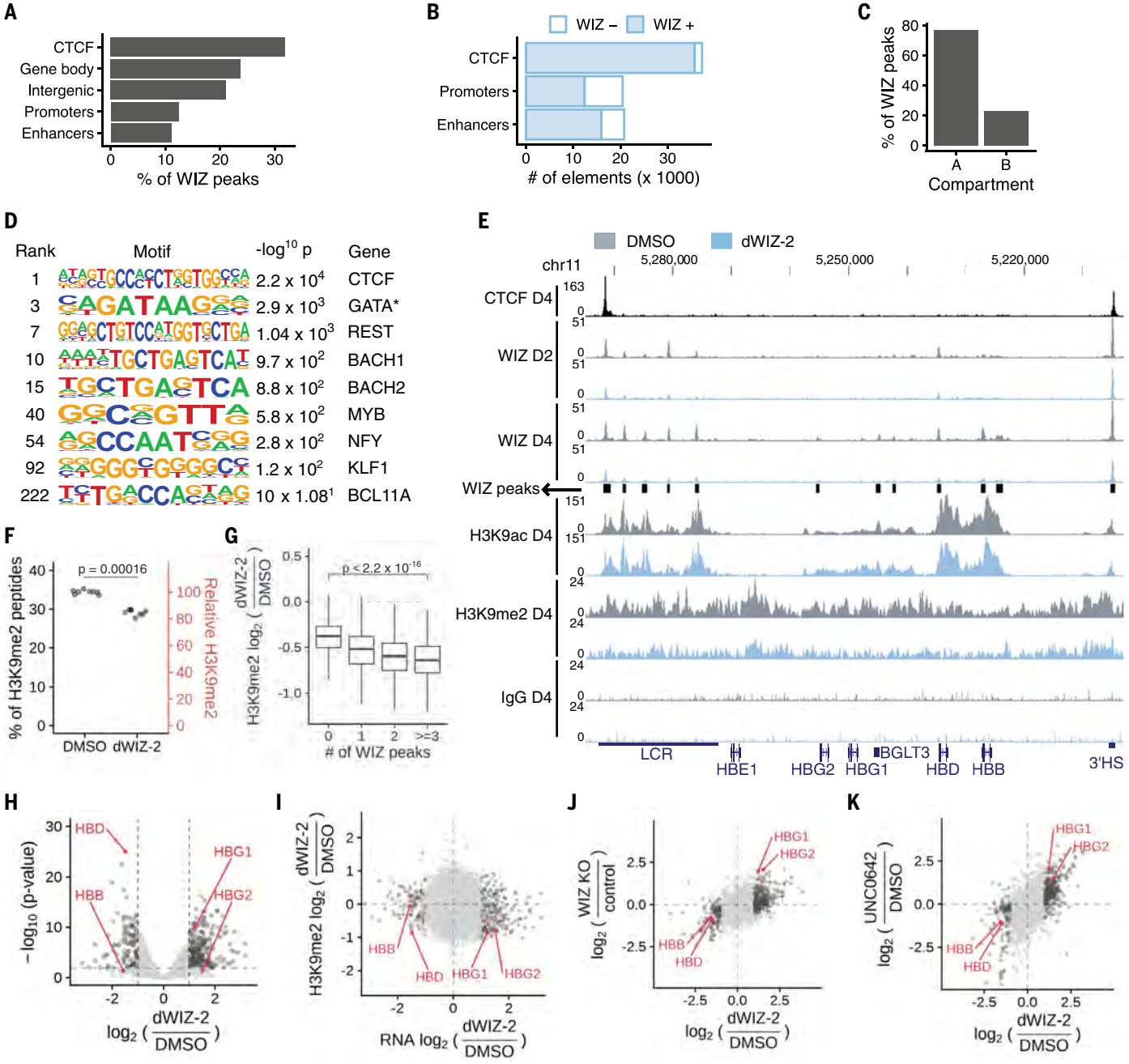

Fig. 5. WIZ CUT&RUN reveals binding in the β-globin locus. (**A**) Distribution of WIZ peaks according to their overlap with gene annotations and genomic regulatory elements. (**B**) Bar plot shows number of CTCF binding sites, promoters, and enhancers in human erythroblasts. The fraction of genome elements with WIZ binding is colored in blue. (**C**) Number of WIZ peaks stratified by their overlap with either active ("A") or inactive ("B") 3D chromatin compartments derived from Hi-C data. (**D**) Table depicting representative cases of the 273 motifs enriched within the WIZ binding sites. Asterisk indicates GATA family TFs. (**E**) Genome browser view of the β-globin locus. The *y*-axis labels indicate the corresponding CUT&RUN profile and differentiation day. WIZ binding sites are indicated as black boxes. At the bottom, the plot shows the location of the genes as well as the LCR and the 3′ hypersensitive site (3′HS). (**F**) Shown are the percentage of total histone H3 peptides (amino acids 9 to 17) detected with a K9me2 modification measured by mass spectrometry. Relative H3K9me2 quantification to the DMSO mean baseline is shown on the right axis. (**G**) For each 10 Kb bin along the genome, the *y* axis shows the ratio (in $\log_2$ scale) between the H3K9me2 CUT&RUN signal in the dWIZ-2–treated erythroblasts and the DMSO-treated erythroblasts. The data are stratified according to the number of WIZ binding sites seen in each genomic 10 Kb bin (*x* axis). (**H**) Volcano plot of the differential gene expression analysis between dWIZ-2–treated erythroblasts and DMSO controls at differentiation day 7. Differentially expressed genes with a twofold change at a FDR of 10% are shown in dark gray. (**I**) Scatterplot showing, for each gene (dots), the change in H3K9me2 signal upon dWIZ-2 treatment at the promoter of the gene (*y* axis) plotted as a function of the gene expression change upon dWIZ-2 treatment. Dots are colored as in (H). (**J**) For each gene (dots) at differentiation day 7, the change in gene expression between the CRISPR *WIZ* KO (*y* axis) and the control is shown as a function of the gene expression change upon dWIZ-2 treatment (*x* axis). Dots are colored as in (H). (**K**) For each gene (dots) at differentiation day 7, the change in gene expression upon 1 μM UNC0642 treatment (EHMT1/2 inhibitor) is shown as a function of the gene expression change upon 10 μM dWIZ-2 treatment (*x* axis). Dots are colored as in (H).

globally as of 2021 (*38*). Emerging paradigms of treatment, such as Cas9-edited or gene-transduced HSPC transplantation, are highly promising (*6*–*8*, *39*), but access to these advances is a barrier to global patient impact (*40*). Oral small-molecule inducers of HbF, if tolerable and efficacious, promise to help address the global unmet need.

Leveraging recent learnings in targeted protein degradation (*11*, *13*, *14*, *41*), we uncovered WIZ as a previously unrecognized and chemically tractable HbF regulator that spares hematopoiesis. In primary human erythroblasts in vitro, CRISPR-Cas9 *WIZ* KO induced comparable levels of HbF and HbF^{+} cells compared with KO of the erythroid +58 enhancer of *BCL11A*, and WIZ degradation induced more HbF compared with HU. Notably, we did not observe cytotoxicity in vitro or in vivo, and there was no dWIZ-2–related toxicity observed in a 4-week cynomolgus monkey study dosed up to 300 mg/kg per day. This mechanism and corresponding phenotype is distinct from HU, which is thought to reactivate HbF through cytotoxicity-induced bone marrow stress (*42*).

Although serendipitously identified by phenotypic screening of a glue degrader library, WIZ is, retrospectively, an appealing target for HbF derepression. Previous work has tied WIZ to heterochromatin silencing by association with EHMT1/2, which have been studied genetically and pharmacologically as targets for HbF induction (*17*, *18*). The effects of acute WIZ degradation share features with EHMT1/2 enzymatic inhibition, including reduced H3K9me2 and overlapping effects on the global transcriptome. It is therefore plausible that WIZ functions as a component of a multiprotein EHMT1/2 repressor complex at the β-globin locus, regulating the expression of HbF through altering chromosomal loop formation (*18*) or by regulating the expression of the lncRNA *BGLT3* (*37*). Whether the modest regional decreases observed in H3K9me2 solely underlie the mechanism of action of WIZ degrader–mediated HbF induction remains to be determined because decreases in H3K9me2 were not uniformly correlated with gene reactivation (Fig. 5I). This selective effect on gene expression suggests the involvement of additional regulatory elements and cell type–specific activation mechanisms at the upregulated genes and/or redundant silencing pathways at the non-derepressed genes.

Curiously, despite overlap in mechanism, WIZ degradation does not exhibit the toxicity observed with previous-generation EHMT1/2 inhibitors (*43*, *44*). Pharmacological profiling across a panel of 319 cell lines revealed markedly less cytotoxicity with WIZ degradation as compared with EHMT1/2 inhibition (fig. S12A). Conceivably, further-optimized EHMT inhibitors may overcome these limitations (*37*). Still, DepMap data across an expansive panel of cell lines demonstrated that *EHMT2* KO exhibited a pan-antiproliferative activity (akin to common essential genes), whereas *WIZ* KO affected only 12 cell lines of 1095 studied (fig. S12B). Although murine KO of *Wiz*, *Ehmt1*, and *Ehmt2* are each lethal, *Wiz* KO pups exhibit perinatal lethality without an impact on assessed tissue proliferation through embryonic day 18.5 (E18.5) (*45*). By contrast, *Ehmt2* KO alone results in growth arrest at E8.5 and early embryonic lethality at E12.5 (*46*). These data suggest that EHMT1/2 and WIZ are not purely redundant in function and that modulating the subunit composition of the complex may differ from inhibiting its enzyme activity. Collectively, our findings suggest that WIZ degradation may be differentiated from EHMT1/2 inhibition, and future studies are needed to delineate the distinct and intersecting functions of these proteins and the relative contributions of different WIZ isoforms. Because WIZ is broadly expressed in multiple tissues and throughout development, the effects of WIZ degradation will also need to be comprehensively assessed preceding and throughout human clinical investigation.

We leveraged phenotypic screening and molecular glue pharmacology to target WIZ, a historically intractable protein target. We contribute dWIZ-1 and dWIZ-2 as chemical probes for mechanistic and translational research and credential WIZ as a therapeutic target for study in SCD.

REFERENCES AND NOTES

1. G. J. Kato *et al*., *Nat. Rev. Dis. Primers* **4**, 18010 (2018).
2. O. S. Platt *et al*., *N. Engl. J. Med.* **330**, 1639–1644 (1994).
3. M. H. Steinberg, *Expert Opin. Ther. Targets* **26**, 347–359 (2022).
4. P. T. McGann, R. E. Ware, *Expert Opin. Drug Saf.* **14**, 1749–1758 (2015).
5. M. de Montalembert *et al*., *Am. J. Hematol.* **96**, 1223–1231 (2021).
6. E. B. Esrick *et al*., *N. Engl. J. Med.* **384**, 205–215 (2021).
7. H. Frangoul *et al*., *N. Engl. J. Med.* **384**, 252–260 (2021).
8. A. Sharma *et al*., *N. Engl. J. Med.* **389**, 820–832 (2023).
9. G. Lettre, D. E. Bauer, *Lancet* **387**, 2554–2564 (2016).
10. M. J. Henley, A. N. Koehler, *Nat. Rev. Drug Discov.* **20**, 669–688 (2021).
11. J. Krönke *et al*., *Nature* **523**, 183–188 (2015).
12. J. Krönke *et al*., *Science* **343**, 301–305 (2014).
13. M. E. Matyskiela *et al*., *Nature* **535**, 252–257 (2016).
14. G. Petzold, E. S. Fischer, N. H. Thomä, *Nature* **532**, 127–130 (2016).
15. E. S. Fischer *et al*., *Nature* **512**, 49–53 (2014).
16. G. Lu *et al*., *Science* **343**, 305–309 (2014).
17. A. Renneville *et al*., *Blood* **126**, 1930–1939 (2015).
18. I. Krivega *et al*., *Blood* **126**, 665–672 (2015).
19. S. E. Meiler *et al*., *Blood* **118**, 1109–1112 (2011).
20. L. A. Moutouh-de Parseval *et al*., *J. Clin. Invest.* **118**, 248–258 (2008).
21. M. Justice, Z. M. Carico, H. C. Stefan, J. M. Dowen, *Cell Rep.* **31**, 107503 (2020).
22. M. Justice, A. F. Bryan, J. C. Limas, J. G. Cook, J. M. Dowen, *BMC Genomics* **23**, 337 (2022).
23. L. Isbel *et al*., *eLife* **5**, e15082 (2016).
24. W. Deng *et al*., *Cell* **149**, 1233–1244 (2012).
25. C. Bian, Q. Chen, X. Yu, *eLife* **4**, e05606 (2015).
26. J. M. Simon *et al*., *J. Biol. Chem.* **290**, 26088–26102 (2015).
27. L. S. Ludwig *et al*., *Cell Rep.* **27**, 3228–3240.e7 (2019).
28. C. Fiorini *et al*., *Am. J. Hematol.* **92**, E513–E519 (2017).
29. D. S. Vinjamur *et al*., *Nat. Genet.* **53**, 719–728 (2021).
30. B. E. McIntosh *et al*., *Stem Cell Reports* **4**, 171–180 (2015).
31. Q. L. Sievers *et al*., *Science* **362**, eaat0572 (2018).
32. E. R. Watson *et al*., *Science* **378**, 549–553 (2022).
33. A. D. Cowan, A. Ciulli, *Annu. Rev. Biochem.* **91**, 295–319 (2022).
34. Z. Kozicka, N. H. Thomä, *Cell Chem. Biol.* **28**, 1032–1047 (2021).
35. O. Humbert, C. W. Peterson, Z. K. Norgaard, S. Radtke, H. P. Kiem, *Mol. Ther. Methods Clin. Dev.* **8**, 75–86 (2017).
36. P. Huang *et al*., *Genes Dev.* **31**, 1704–1713 (2017).
37. S. Takase *et al*., *Nat. Commun.* **14**, 23 (2023).
38. GBD 2021 Sickle Cell Disease Collaborators, *Lancet Haematol.* **10**, e585–e599 (2023).
39. J. Kanter *et al*., *N. Engl. J. Med.* **386**, 617–628 (2022).
40. A. A. Abraham, J. F. Tisdale, *Blood* **138**, 932–941 (2021).
41. S. Bonazzi *et al*., *Cell Chem. Biol.* **30**, 235–247.e12 (2023).
42. D. Lavelle, J. DeSimone, P. Heller, D. Zwiers, L. Hall, *Blood* **67**, 1083–1089 (1986).
43. S. Kubicek *et al*., *Mol. Cell* **25**, 473–481 (2007).
44. M. Vedadi *et al*., *Nat. Chem. Biol.* **7**, 566–574 (2011).
45. I. Bukova *et al*., *Front. Cell Dev. Biol.* **9**, 620692 (2021).
46. M. Tachibana *et al*., *Genes Dev.* **16**, 1779–1791 (2002).

ACKNOWLEDGMENTS

The authors thank many Novartis colleagues whose efforts enabled this work: J. Snead and J. Joslin for development of the phenotypic screening assay; J. McKenna, R. Tichkule, K. Yamada, and the library build team; R. Maher and J. Reece-Hoyes for vector construction; F. Xu for seminal proteomics studies and T. Rejtar for proteomics informatics expertise; F. Tang for analysis of published expression datasets; M. Zambrowski for determination of compound stability; N. Charles for immunoblot analysis; J. Blankenship for advice in generating the WIZ antibody; B. Leon for protein purification; P. Zhang for flow cytometry support; D. Lubicka for formulations; J. Wang, M. Hossain, Q. Zhang, Y. Sun, G. Wussler, G. Boynton, A. McCall, D. Moreton, D. Basta, A. Taylor, D. Manning, E. Cullins, E. Mondesir, M. Seeraj, and T. Gil for assistance with the humanized mouse studies; S. Miranda, C. Kos, D. Walker, and A. Piaia for cynomolgus monkey study support and analysis; G. Boynton for analysis of cynomolgus mRNA samples; M. Shum, P. Aspesi, J. Ambrose, R. Newcombe, M. Jones, L. Barys, and P. Mapa for cell line profiling; P. Ashcroft, J. Manning, A. Knight, and T. Nicholson for insightful discussions; R. McDonald, J. Shulok, U. Naumann, R. Jain, J. Tallarico, K. Briner, and P. Tarsa for guidance and support; and M. Hossain, A. Tovy, E. Furutani, W. Forrester, and G. Hollingworth for careful reading and editing of the manuscript. The authors also thank the healthy and SCD donors who donated samples to support these studies. X-ray data were collected at the Advanced Photon Source beamline ID17. **Funding:** This study was supported by Novartis Biomedical Research. **Author contributions:** Conceptualization: P.Y.T., R.E.J.B., J.M.S., and J.E.B. Formal analysis: P.Y.T., S.B., E.A., A.E.H., N.P., A.R., B.D.F., M.S.B., S.C., A.H., J.S.C., A.B., D.D., J.L., M.C.C., X.Ma, J.T., M.A., and S.W.B. Investigation: P.Y.T., S.B., N.M.T., E.A., A.E.H., N.P., F.W., M.S.B., J.Wan., A.H., A.B., D.D., J.L., E.O., N.F.W., and J.K. Methodology: P.Y.T., S.B., J.R.K., N.M.T., E.A., A.E.H., N.P., A.R., B.D.F., X.Ma, S.C., W.N., J.S.C., J.P., D.D., J.L., M.C.C., X.Mao, C.C.S., and R.T. Project administration: P.Y.T., J.R.K., and N.A.S. Supervision: N.A.D., A.W.P., J.Wag., T.B., G.D., and S.C.S. Writing – original draft: P.Y.T., A.R., B.D.F., and M.C.C. Writing – review & editing: P.Y.T., E.A., A.E.H., A.R., B.D.F., and J.E.B. **Competing interests:** All authors are past or current employees of Novartis. J.E.B. is a prior executive and remains a shareholder of Novartis AG; he is presently the EVP R&D and CSO of Amgen and a shareholder. Some of the authors have patents related to this work: WO2021124172, 3-(5-methoxy-1-oxoisoindolin-2-yl)piperidine-2,6-dione derivatives and uses thereof (J.S.C., N.A.D., J.R.K., A.W.P., N.M.T., and P.Y.T.) and WO2021123920, Composition and methods for the treatment of hemoglobinopathies (M.S.B., J.E.B., J.S.C., S.C.S., P.Y.T., N.A.D., J.R.K., and N.M.T.). The authors declare no other competing interests. **Data and materials availability:** Structural data have been deposited in the RCSB Protein Data Bank (PDB) (https://www.rcsb.org/). The PDB accession code for the human DDB1:CRBN:dWIZ-1:WIZ(ZF7) x-ray costructure is 8TZX. The RNA-seq and CUT&RUN data have been deposited to GEO (GSE247096) and ArrayExpress (E-MTAB-13890). The mass spectrometry proteomics data have been deposited to the ProteomeXchange Consortium via the PRIDE partner repository with the dataset identifier PXD046433. The code to reproduce the panels from Fig. 5 and fig. S11 is available in the Novartis Github organization under the repository dWIZ (https://

github.com/Novartis/dWIZGenomics). All compounds and reagents can be obtained through a material transfer agreement from Novartis by submitting a request through the following portal: https://www.cybergrants.com/pls/cybergrants/quiz.display_question?x_gm_id=2932&x_quiz_id=9952.

SUPPLEMENTARY MATERIALS

science.org/doi/10.1126/science.adk6129
Materials and Methods
Figs. S1 to S12
Tables S1 to S4
References (*47*–*72*)
MDAR Reproducibility Checklist

Submitted 27 October 2023; accepted 5 May 2024
10.1126/science.adk6129